Probing the *Paracoccus denitrificans* Cytochrome c_1−Cytochrome c_{552} Interaction by Mutagenesis and Fast Kinetics[†]

Julia Janzon,[*,‡] Quan Yuan,[§] Francesco Malatesta,[∥] Petra Hellwig,[⊥] Bernd Ludwig,[‡,+] Bill Durham,[§] and Francis Millett[§]

Molecular Genetics, Institute of Biochemistry, Biocentre Goethe-University, 60438 Frankfurt/Main, Germany, Department of Chemistry and Biochemistry, University of Arkansas, Fayetteville, Arkansas 72701, Department of Pure and Applied Biology, University of L'Aquila, I-67010 L'Aquila, Italy, Institut de Chimie-UMR 7177, Laboratoire de spectroscopie et électrochimie des biomolécules, Université Louis Pasteur, rue Blaise Pascal, 67070 Strasbourg, France, and Cluster of Excellence "Macromolecular Complexes", Goethe-University, 60438 Frankfurt/Main, Germany

Received May 19, 2008; Revised Manuscript Received October 13, 2008

ABSTRACT: Electron transfer (ET) between *Paracoccus denitrificans* cytochrome (cyt) c_1 and cytochrome c_{552} was studied using the soluble redox fragments cyt c_{1CF} and cyt c_{552F}. A new ruthenium cyt c_{552F} derivative labeled at C23 (Ru_z-23-c_{552F}) was designed to measure rapid electron transfer with cyt c_{1CF} in the physiological direction using flash photolysis. The bimolecular rate constant k_{12} decreased rapidly with ionic strength above 40 mM, consistent with a diffusional process guided by long-range electrostatic interactions between the two proteins. However, a new kinetic phase was detected at an ionic strength of <35 mM with the ruthenium photoexcitation technique in which k_{12} became very rapid (3×10^9 M^{-1} s^{-1}) and nearly independent of ionic strength, suggesting that the reaction became so fast that it was controlled by short-range diffusion along the protein surfaces guided by hydrophobic interactions. These results are consistent with a two-step model for formation of the final encounter complex. No intracomplex electron transfer between Ru_z-23-c_{552F} and c_{1CF} was observed even at the lowest ionic strength, indicating that the dissociation constant of the complex was >30 μM. On the other hand, the ruthenium-labeled yeast cytochrome *c* derivative Ru_z-39-*Cc* formed a tight 1:1 complex with cyt c_{1CF} at ionic strengths of <60 mM with an intracomplex electron transfer rate constant of 50000 s^{-1}. A group of cyt c_{1CF} variants in the presumed docking site were generated on the basis of information from the yeast cyt bc_1−cyt *c* cocrystal structure. Kinetic analysis of cyt c_{1CF} mutants located near the heme crevice provided preliminary identification of the interaction site for cyt c_{552F} and suggested that formation of the encounter complex is guided primarily by the overall electrostatic surface potential rather than by defined ions.

The mitochondrial respiratory chain consists of four redox protein complexes that transfer electrons from NADH (or $FADH_2$) to the terminal electron acceptor dioxygen. The free energy of these redox processes is used by three of the four transmembrane complexes to translocate protons across the inner mitochondrial membrane, thus generating an electrochemical proton gradient utilized by the ATP synthase to phosphorylate ADP (*1*). The cytochrome bc_1 complex represents the central core of the aerobic respiratory chain of eukaryotes and many prokaryotes. In bacteria, its simplest version consists of only the cofactor-containing subunits (*2*) [the Rieske iron−sulfur protein (ISP), cytochrome *b* (cyt[1] *b*), and cytochrome c_1 (cyt c_1)], whereas eukaryotes contain up to eight additional subunits, which may be involved in complex stability, assembly, or regulation (*3*−*6*).

The bc_1 complex of yeast mitochondria has been cocrystallized with its bound substrate, soluble cytochrome *c*, revealing insight into the cyt c_1−cyt *c* interactions (*7*−*9*). A small, compact, mainly apolar binding site was identified, where direct contacts are mediated by hydrophobic interactions and a central cation−π interaction, with only two potential polar interactions. Similar results were obtained for several other cytochrome *c* redox complexes from different organisms using cocrystallization and X-ray approaches,

[†] This work was supported by Deutsche Forschungsgemeinschaft (SFB 472) and by NIH Grants GM20488 (F. Millett and B.D.) and P20 RR15569.

* To whom correspondence should be addressed. Fax: (+49) 69-798-29515. Phone: (+49) 69-798-29127. E-mail: Janzon@nmr.uni-frankfurt.de.

[‡] Biocentre Goethe-University.

[§] University of Arkansas.

[∥] University of L'Aquila.

[⊥] Université Louis Pasteur 4.

[+] Goethe-University.

[1] Abbreviations: c_{1CF}, soluble cytochrome c_1 core fragment of *Paracoccus denitrificans*; c_{552F}, soluble cytochrome c_{552} fragment of *P. denitrificans*; cyt, cytochrome; DSC, double sector cuvette; ET, electron transfer; ISD, ionic strength dependency; FP, flash photolysis; *Pd*, *P. denitrificans*; Ru_z, Ru(2,2′-bipyrazine)$_2$(4-bromomethyl-4′-methyl-2,2′-bipyridine); Ru_z-23-c_{552F}, *Pd* cytochrome c_{552F} with surface asparagine 23 mutated to cysteine (N23C) and covalently attached to Ru_z; Ru_z-39-*Cc*, yeast isocytochrome *c* with cysteine 102 mutated to threonine (C102T) and an introduced surface cysteine in position 39 (H39C), covalently attached to Ru_z; *Sc*, *Saccharomyces cerevisiae*; SF, stopped-flow; WT, wild-type.

10.1021/bi800932c CCC: $40.75
Published on Web 11/12/2008

as well as chemical shift perturbation mapping NMR experiments (*8, 10*−*13*) and EPR measurements (*14*).

In contrast to this, mutagenesis and functional kinetic studies of the transient electron transfer (ET) reactions between cyt c_1 and cyt *c* revealed a clear electrostatic component. Acidic residues located around the heme cleft on cyt c_1 as well as lysine residues surrounding the heme crevice on cyt *c* were found to contribute to the Coulombic interaction (*15*−*19*). These results led to a two-step model for transient ET reactions describing the association of the two redox partners. Driven by long-range electrostatic interactions, the redox partners approach each other, resulting in the formation of an encounter complex, which represents an ensemble of different relative orientations of both redox partners. Diffusion along the protein surfaces subsequently leads to the fine adjustment of both redox partners mediated by short-range hydrophobic interactions to yield the efficient complex, allowing fast ET (*20*−*25*).

The soil bacterium *Paracoccus denitrificans* expresses aerobic respiratory chain complexes which are homologous to its mitochondrial counterparts yet are much simpler in subunit composition, thus making *P. denitrificans* a suitable model system for mitochondrial ET processes. The *Paracoccus* bc_1 complex consists of just three redox-active subunits (*26*). Cytochrome c_1 shows a tripartite domain structure (*27*). An N-terminal, highly acidic domain unique to *Paracoccus* is proposed, due to its strongly negative charge, to mimic the acidic hinge protein in the bovine bc_1 complex (*28*) or subunit QCR6 in the yeast complex (*6*). The central core domain carries the covalently attached *c*-type heme group and is followed by the C-terminal sequence for the membrane anchor. Electrons are passed from cyt c_1 to membrane-bound cyt c_{552}, which has been shown to be the genuine electron acceptor of the bc_1 complex (*29*). An electrostatic contribution to the interactions between cyt c_{552} and cyt c_1 has been deduced from kinetic investigations using genetically engineered soluble modules of both redox partners. The soluble cytochrome c_1 core fragment (cyt c_{1CF}) (*27*) consists of only the central core domain, lacking the acidic domain as well as the membrane anchor. The soluble cytochrome c_{552} fragment (cyt c_{552F}) (*30*) contains only the C-terminal hydrophilic heme-carrying domain without the N-terminal membrane anchor and linker region. Both fragments can be regarded as minimal redox units of the native cytochromes, providing the advantage of simplified experimental design as no detergents are necessary to keep the cytochromes soluble. Moreover, the ET reaction of interest is not influenced by subsequent ET events or energy transduction steps, as in the case of redox complexes.

The transient nature of ET reactions between redox proteins has previously been studied using stopped-flow techniques (*21, 22, 24, 27, 31*−*33*) and EPR (*14*). In particular, the pre-steady state kinetics of terminal ET processes in the aerobic respiratory chains of *P. denitrificans* and *Thermus thermophilus* have been investigated using soluble fragments of membrane-bound redox proteins and soluble cytochrome *c* species (*21, 22, 24, 31*−*33*).

A ruthenium flash photolysis method for characterizing both intracomplex and bimolecular ET between redox partners with microsecond time resolution, as well as ET within redox protein complexes such as the cyt bc_1 complex (*32*−*39*), has been developed. A photoexcitable ruthenium complex is either covalently attached to one redox partner or bound by electrostatic interactions (*3, 34*−*36*). Photoexcitation of Ru(II) to Ru(II*) rapidly reduces or oxidizes the neighboring heme group and induces subsequent ET events. The development and synthesis of ruthenium complexes with differing redox properties allowed the determination of ET processes in a number of redox systems (*3*), including intracomplex ET within the bc_1 complex of different organisms (*3, 34*−*36*) and the intermolecular reaction between cyt *c* and cyt c_1 of the bc_1 complex (*3, 36*).

Here we present the functional and dynamic characterization of the ET reaction between *P. denitrificans* cyt c_{1CF} and cyt c_{552F} using both stopped-flow spectroscopy and ruthenium photoexcitation techniques. To study the ET reaction between cyt c_{1CF} and cyt c_{552F} in the physiological direction, Ru_z-23-c_{552F} was prepared by covalently attaching the photoexcitable ruthenium compound Ru(2,2′-bipyrazine)$_2$(4-bromomethyl-4′-methyl-2,2′-bipyridine) (Ru_z) (*3*) to the single cysteine introduced on the surface of cyt c_{552F}N23C. The second-order rate constant of the reaction of Ru_z-23-c_{552F} with cyt c_{1CF} is the same as that of unlabeled cyt c_{552F} at an ionic strength of 200 mM, indicating that the ruthenium label does not affect the reaction under these conditions. The high time resolution of the ruthenium method allowed extension of the kinetic studies to low ionic strengths, where evidence for a two-step mechanism was observed.

To determine the interaction interface on *P. denitrificans* cyt c_1 for cyt c_{552}, a series of cyt c_{1CF} variants in the presumed docking site were prepared. The yeast cyt bc_1−cyt *c* cocrystal structure (*7*−*9*) was used in combination with sequence alignment and structural modeling to identify residues in the putative binding site of *P. denitrificans* cyt c_{1CF}, since structures of neither *P. denitrificans* cyt c_1 nor the c_1−c_{552} complex are available. The side chain residues were varied in bulk, polarity, or charge, and the kinetics of the reactions of the cyt c_{1CF} mutants with cyt c_{552F}, Ru_z-23-c_{552F}, and yeast Ru_z-39-*Cc* were examined.

EXPERIMENTAL PROCEDURES

Site-Directed Mutagenesis, Heterologous Expression, and Purification Procedures. Site-directed mutagenesis was performed using the QuikChange (Stratagene) or Altered sites (Promega) mutagenesis kits. pET-22b(+) (Novagen) and pAlter-Ex1 (Stratagene) served as templates for the cyt c_{1CF} mutagenesis reaction, with the cyt c_{1CF} gene cloned via *Nco*I and *Hin*dIII into the multiple cloning sites (for details, see ref *27*).

For introducing the surface cysteine (N23C) into cyt c_{552F}, pBR2 (*30*) was taken as the template. The following primers were used (mutagenic triplet in bold): E243K, 5′-C TTG CAG GTC TAT A*CC* **AAG** GTC TGC TCG G*CC* TGC-3′; V244Q, 5′-CAG GTC TAT A*CC* GAG **CAG** TGC TCG G*CC* TGC CAC-3′; V244Q_rev, 5′-GTG GCA GGC CGA GCA GGT **CTC** GGT ATA GAC CTG-3′; V244T, 5′-CAG GTC TAT A*CC* GAG **A*CC*** TGC TGC G*CC* TGC CAC-3′; V244T_rev, 5′-GTG GCA GGC CGA GCA **GGT** CTC GGT ATA GAC CTG-3′; A247N, 5′-A*CC* GAG GTC TGC TCG **AAC** TGC CAC GGC CTG CGC-3′; A247N_rev, 5′-GCG CAG G*CC* GTG GCA **GTT** CGA GCA GAC CTC GGT-3′; A314S, 5′-GAC CTG TCG CTG ATG **TCA** AAG GCG CGC G*CC* GGG-3′; A314S_rev, 5′-*CC*C GGC GCG

CGC CTT **TGA** CAT CAG CGA CAG GTC-3′; K315E, 5′-CTG TCG CTG ATG G*CC* **GAG** GCG CGC G*CC* GGG TTC-3′; K315E_rev, 5′-GAA *CC*C GGC GCG CGC **CTC** GGC CAT CAG CGA CAG-3′; K315T, 5′-CTG TCG CTG ATG G*CC* **ACG** GCG CGC G*CC* GGG TTC-3′; K315T_rev, 5′-GAA *CC*C GGC GCG CGC **CGT** GGC CAT CAG CGA CAG-3′; G319A, 5′-G*CC* AAG GCG CGC G*CC* **GCG** TTC CAT GGC *CC*C TAC-3′; G319A_rev, 5′-GTA GGG G*CC* ATG GAA **CGC** GGC GCG CGC CTT GGC-3′; S378A, 5′-ATG GCG GCG *CC*C CTC **G*CC*** GAC GAC CAG GTC A*CC*-3′; S378A_rev, 5′-GGT GAC CTG GTC GTC **GGC** GAG GGG CGC CGC CAT-3′; Q381V, 5′-*CC*C CTC AGC GAC GAC **GTG** GTC A*CC* TAT GAG GAT-3′; Q381V_rev, 5′-ATC CTC ATA GGT GAC **CAC** GTC GTC GCT GAG GGG-3′; T383C, 5′-AGC GAC GAC CAG GTC **TGC** TAT GAG GAT GGC A*CC*-3′; c_{552F}_N23C, 5′-AAG CTG GAC GGC **TGC** GAT GGC GTC GGC *CC*G-3′; N23C_rev, 5′-CGG G*CC* GAC G*CC* ATC **GCA** G*CC* GTC CAG GTT-3′.

Cytochrome c_{552F} was expressed and purified as described by Reincke et al. (*30*). Cytochrome c_{1CF} and mutants were expressed heterologously in *Escherichia coli* BL21(DE3) using pET-22b(+) (both Novagen) as the IPTG-inducible expression plasmid, which provides the *pel*B leader sequence for periplasm transport of the apoprotein. Cotransformation with heme maturation plasmid pEC86 (*37*) achieved efficient incorporation of the cofactor into the cytochrome. Cells were incubated at 37 °C and harvested 3−4 h after induction with 0.4 mM IPTG, yielding ~4 mg of cyt c_{1CF} per liter of culture medium. The periplasm was prepared (*38*), and the cytochromes were purified via ion exchange chromatography [Q-Sepharose *fast flow* (Amersham Bioscience) with 50 mM Tris-HCl (pH 8.0), 50 mM NaCl, and 2 mM EDTA; with a NaCl gradient from 50 to 500 mM] and gel filtration [Sephacryl S-100 (Amersham Bioscience) with 50 mM Tris-HCl (pH 8.0), 150 mM NaCl, and 2 mM EDTA]. Purification steps were followed by SDS−PAGE (*39*) and Western blot analysis. Correct heme incorporation was demonstrated by heme staining (*40*), charge transfer, and absorption (Supplement 1 of the Supporting Information) redox difference spectra. In addition, the X-ray and NMR structures of cyt c_{552F} in both redox states are known (*30, 41*). For precise cytochrome concentrations during the stopped-flow and laser flash experiments, extinction coefficients of each cyt c_{1CF} mutant were determined by pyridine hemochrome spectra (*42*) (see Supplement 2 of the Supporting Information). Additionally, the redox potentials of wild-type cyt c_{1CF} and its mutants were determined by redox titrations versus the standard hydrogen electrode at pH 7.0 (SHE′) (see Supplement 2 of the Supporting Information).

Pre-Steady State Stopped-Flow Kinetics. To bypass the problem of spectral overlap, wavelengths at which the ET reactions between the cytochromes could be detected had to be found. This was achieved by recording difference spectra using double sector cuvettes (DSCs) (for details, see ref *27*). The peaks and troughs of the DSC spectra in the Soret and α-region display those wavelengths of minimal spectral overlap and maximal signal amplitude (see Supplement 2 of the Supporting Information). All kinetic experiments were carried out using a thermostated Applied Photophysics (Leatherhead, U.K.) stopped-flow apparatus with a 1 cm observation chamber. Nitrogen-flushed Tris-HCl buffer was used [20 mM Tris-HCl (pH 8.0), 20 mM KCl, and 1 mM EDTA], and the ionic strength was varied via addition of appropriate amounts of solid KCl. Cyt c_{1CF} was prereduced with 0.5 mM ascorbate for at least 10 min before the measurements in a reaction sufficiently slow not to interfere with the ET reaction of interest (*27*). ET kinetics were studied in the physiological forward direction from cyt c_{1CF} to cyt c_{552F} at 48 °C. At least three kinetic traces were averaged and fitted, taking into account the prevalent non-pseudo-first-order conditions (for details, see ref *27*). Bimolecular rate constants were plotted according to the Brønsted equation (*43*) to determine the ionic strength dependence of the reaction rates. Data fitting was performed using Origin 7.5 (OriginLab Corp.). The standard deviation of the fitted parameters was <10%.

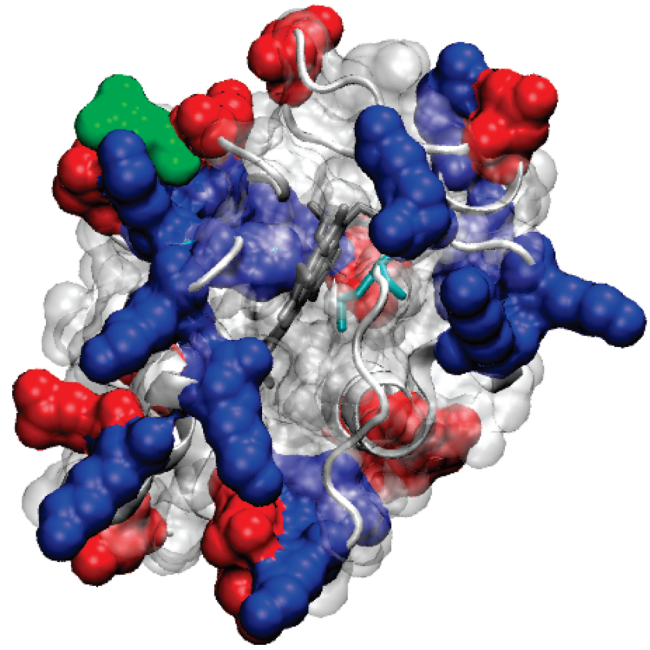

FIGURE 1: Surface representation of *Pd* cyt c_{552F} [PDB entry 1QL4 (*30*)] viewed toward the heme crevice and potential interaction interface with cyt c_{1CF}. The overall surface (white) is partially transparent, allowing visualization of the heme group (gray), the distal heme ligand Met78 (cyan), and the cytochrome backbone fold (light gray). Basic residues (blue) surround the heme cleft, whereas the acidic residues (red) are located at its periphery or on the c_{552F} reverse side. Asparagine 23, which was mutated to cysteine and covalently attached to the ruthenium complex in Ru_z-23-c_{552F}, is colored green.

Preparation of Ru_z-23-c_{552F}. Site-directed mutagenesis was used to introduce a single cysteine at residue N23 on the surface of cyt c_{552F} remote from the putative reaction site with cyt c_1 (Figure 1). The ruthenium reagent Ru(2,2′-bipyrazine)$_2$(4-bromomethyl-4′-methyl-2,2′-bipyridine) (Ru_z) is highly selective for labeling only cysteine residues under the conditions used (*39*). N23C cyt c_{552F} (1.4×10^{-7} mol) was treated with a 10-fold molar excess of dithiothreitol (DTT) to reduce the cysteine and concentrated and exchanged to 0.7 mM in a volume of 200 μL of 50 mM sodium borate buffer (pH 9.0) using a Centricon Ultracel YM-10 concentrator. A 2-fold molar excess of DTT was added to the anaerobic solution of the protein, followed by the addition of a 3-fold molar excess of Ru(2,2′-bipyrazine)$_2$(4-bromomethyl-4′-methyl-2,2′-bipyridine) with stirring. Ruthenium labeling was continued for 12−14 h in the dark under anaerobic conditions at room temperature. The reaction

mixture was then exchanged in 5 mM sodium phosphate buffer (pH 7.0) to lower the ionic strength and applied to a 5 mm × 50 mm DE53 column equilibrated with 5 mM sodium phosphate (pH 7.0). Only unlabeled N23C cyt c_{552F} strongly bound to the column while most of the labeled protein was eluted with 5 mM phosphate buffer. Ru_z-23-c_{552F} was purified by HPLC on a 1.5 cm × 30 cm high-resolution DEAE-52 column which can separate Ru_z-23-c_{552F} from possible impurities. Before the sample was loaded on the HPLC column, DTT (or ascorbate) was added to keep Ru_z-23-c_{552F} reduced and bound to the anion exchange column. A single major peak eluted off the DEAE-52 column which had a UV−visible spectrum equal to the sum of 1 equiv of cyt c_{552F}-N23C and 1 equiv of Ru_z. The purified Ru_z-23-c_{552F} was exchanged three times with 5 mM sodium phosphate buffer (pH 7.0), then concentrated, and frozen at −80 °C. The overall yield of Ru_z-23-c_{552F} was ∼30%, and most of the remaining 70% was unlabeled N23C cyt c_{552F}.

Flash Photolysis Experiments. Transient absorbance measurements of ET between Ru_z-23-c_{552F} and cyt c_{1CF} were carried out using a phase R model DL 1400 flash lamp-pumped dye laser generating a 480 nm excitation light pulse with a duration of 0.5 μs and a detection system described by Heacock et al. (*44*). Solutions contained ∼5 μM Ru_z-23-c_{552F} and 1−20 μM cyt c_{1CF} in 300 μL of 10 mM Tris-HCl buffer (pH 8.0) in semimicro glass cuvettes. Addition of 0.1−1.1 mM sodium ascorbate and 2 μM *N*,*N*,*N*′,*N*′-tetramethylphenylenediamine (TMPD) achieved reduction of the heme groups. The sacrificial oxidant paraquat in oxygen-saturated buffer was used to reoxidize Ru(I) to Ru(II). Ionic strength conditions were varied by the addition of the appropriate volume of a 2 M KCl stock solution. The ET reaction was monitored at 550 and 558 nm. The reaction between yeast Ru-39-*Cc* and cyt c_{1CF} was studied under the same conditions except that 5 mM sodium phosphate (pH 7.0) was used as the buffer. All absorbance transients were analyzed using the KINFIT kinetics program obtained from Online Instrument System Inc. Absorbance spectra were obtained with a Hewlett-Packard 8452A diode array spectrophotometer.

RESULTS AND DISCUSSION

Our aim was to characterize the ET reaction between *Pd* cyt c_{1CF} and cyt c_{552F} and identify those residues on cyt c_1 which contribute to the reaction. Since no structural data of *Pd* cyt c_1 or its complex with cyt c_{552} are available, the yeast cyt bc_1−cyt *c* cocomplex structure (*6*−*9*) was used as a guide for identifying putative residues at the binding domain. Although the yeast cyt bc_1 complex shows a bell-shaped ionic strength dependence of activity (*45*), the cyt bc_1−cyt *c* cocomplex structure revealed a small compact contact site between cyt c_1 and cyt *c* with direct interactions mediated primarily by apolar contacts and a central cation−π interaction between Phe230 of cyt c_1 and Arg13 of cyt *c*. No salt bridges or hydrogen bonds were observed within this nonpolar contact area (*9*), but it is surrounded by a semicircle of oppositely charged ion pairs, which are not in close contact, thus mediating weak electrostatic interactions (*9*). We identified corresponding residues on *Pd* cyt c_1 by sequence alignment and structural modeling approaches and varied the bulk, charge, or polarity of these residues by site-directed mutagenesis. The biochemical, spectral, and redox properties of the mutant proteins were fully characterized. To identify the interaction domain, the kinetics of the reaction between the cyt c_{1CF} mutants and cyt c_{552F} was studied using both the high-speed ruthenium flash photolysis method and stopped-flow spectroscopy.

Table 1: Amino Acid Positions on cyt c_1 of the Yeast cyt bc_1−cyt *c* Cocomplex Crystal [PDB entry 1KYO (*8*)] Mediating Direct Interactions with cyt *c*, Corresponding Residues on *Pd* cyt c_1, and Site-Directed Mutations

amino acid position in yeast cyt c_1	amino acid position in *Pd* cyt c_1	mutation(s)
E99[a]	E243	E243K
V100[a]	V244	V244Q/T
A103	A247	A247N
A164	A314	A314S
	K315	K315E/T
A168	G319	G319A
F230	S378	S378A
M233	Q381	Q381V
E235	T383	T383C

[a] E99 and V100 do not show direct interactions in the yeast cocomplex but are surface exposed in the *Sc* structure and were additionally chosen for mutagenesis.

Generation of the cyt c_{1CF} Mutants and Redox Biochemical Characterization. Identification of the corresponding residues in *Pd* cyt c_1 was achieved by performing a sequence alignment [ClustalW (*46*)], using the cyt c_1 sequences of *Rhodobacter capsulatus* (*Rc*), *Rhodobacter sphaeroides* (*Rs*), *Pd*, *Saccharomyces cerevisiae* (*Sc*), and *Bos taurus* (*Bt*) (see Supplement 3 of the Supporting Information). The alignment revealed a couple of gaps and sequence insertions between the pro- and eukaryotic sequences, as well as between the *Pd* and *Rhodobacter* sequences, rendering the search for the corresponding cyt c_1 residues challenging. In case an aligned position was ambiguous, additional alternative mutagenesis positions were chosen. cyt c_1 positions mediating direct interactions with cyt *c* within the yeast cocrystal, the corresponding residues in the *Pd* cyt c_1, and site-directed mutations are listed in Table 1.

In addition, the *Pd* cyt c_1 sequence was modeled onto the yeast cytochrome c_1 structure [PDB entry 1KYO (*8*)] using different approaches [Swissmodell (*47*), Jigsaw3D (*48*), and Esypred (*49*)] to determine if the chosen amino acids of *Paracoccus* cyt c_1 are located at similar positions in the putative structure and show a similar orientation toward the potential interaction interface as in the yeast cocomplex (see Figure 2 for the cyt c_{1CF} Swissmodel structure). The overall modeled cyt c_{1CF} backbone fold was nearly identical to that of PDB entry 1KYO, displaying deviations only in the loop regions in agreement with the gaps and insertions in the sequence alignment. Mutated side chain positions showed a similar location and orientation within the different structural models as well as the yeast cyt c_1 structure. The heme cleft is surrounded by surface-exposed acidic residues in a circular arrangement, which may be responsible for long-range electrostatic steering of both redox partners to form an encounter complex (see Figure 1 for the complementary heme hemisphere of cyt c_{552F}).

On the basis of the sequence alignment and structural models, the mutated positions were grouped into three regions (region I−III; see Figure 2). Region I contains mutations E243K, V244Q, V244T, and A247N, which are

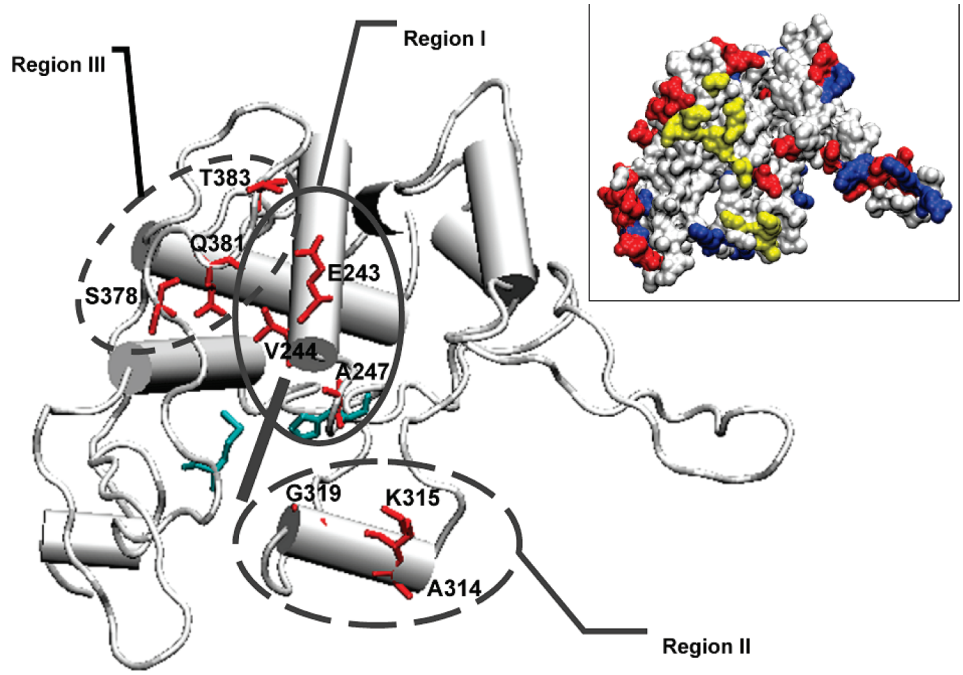

FIGURE 2: *Pd* cyt c_{1CF} sequence modeled onto the yeast *Sc* cyt c_1 structure [PDB entry 1KYO (*8*)] using Swissmodell (*47*). The view is toward the heme crevice and membrane plane along the transmembrane helix (TMH). Regions I−III as designated (for further details, see the text): red for positions for mutagenesis, cyan for axial and distal heme ligands (M373 and H249), and a dark gray bar for the simulated heme group. The inset shows a cyt c_{1CF} surface representation (same orientation as in the main panel). Mutated positions are colored yellow and basic residues blue. Acidic residues (red) form a distant ring around the heme cleft.

all located within or directly preceding the heme binding motif CXXCH in the amino acid sequence. This region is positioned directly above the heme crevice when viewed onto the membrane plane along the transmembrane helix (TMH) present in native cyt c_1. The position of α-helical region II is ambiguous, as obtained by the different structural models, and contains the mutations A314S, K315E/T, and G319A, all positions highly conserved in prokaryotes. Its most likely localization is below the heme crevice. Region III is located on the left in vicinity to region I and seems to be conserved in all structural models. As indicated by the sequence alignment, S378 within region III is the residue corresponding to F230 of yeast, which is seen in that structure (*8*) to mediate the cation−π interaction. Residue Q381 corresponds to M233.

Variants were generated by site-directed mutagenesis, expressed heterologously in *E. coli*, purified, and biochemically characterized by SDS−PAGE, Western blot analysis, and heme staining, confirming that all mutant proteins were identical to wild-type c_{1CF} (data not shown).

Stopped-Flow Kinetics of the ET Reaction between Wild-Type cyt c_{1CF} and cyt c_{552F}. The ET reaction between WT cyt c_{1CF} and cyt c_{552F} using pre-steady state stopped-flow techniques previously described (*27*) followed an optimized protocol dealing with the problems of spectral overlap, heme autoxidation, and non-pseudo-first-order conditions. Using soluble modules of redox proteins of respiratory chain complexes as models for elucidation of electron transport mechanisms offers the advantage of simplified experimental procedures, as no detergent is required to keep the cytochromes in solution. Moreover, only the ET reaction of interest is followed, and kinetic interference by subsequent internal ET or energy transduction steps is circumvented. However, it should be kept in mind that the reactions of soluble fragments in solution provide a higher degree of diffusional freedom compared to the reaction of membrane-anchored cyt c_{552} with cyt c_1 in the transmembrane bc_1 complex, where the directionality of the ET interactions is physically much more restricted. By performing the kinetics at 8 °C, we were able to resolve the bimolecular ET reaction down to an ionic strength of 70 mM. The second-order rate constant (k_{12}) was 2.3×10^8 M^{-1} s^{-1} at an ionic strength of 70 mM, decreasing to 2.3×10^6 M^{-1} s^{-1} at an ionic strength of 320 mM (Figure 5). Plotting the logarithm of the bimolecular rate constants versus the square root of the ionic strength according to the Brønsted law (*43*) yielded a Z_AZ_B parameter of −4.0, consistent with a diffusional process mediated by electrostatic interactions between the two proteins. Although the Brønsted equation is strictly applicable only to small molecules at low ionic strengths, it has been widely used as an empirical measure of the importance of electrostatic interactions between redox proteins (*28, 50*). However, it is not possible to determine whether the reaction studied here is fully or only partially diffusion-limited, and the Brønsted parameter should be considered strictly empirical. A Z_AZ_B parameter of −4.0 has also been previously found for the ET reaction between *Paracoccus* cyt c_{552} and the Cu_A fragment of the aa_3 oxidase (*24, 32*), suggesting that cyt c_{552} binds to both cyt c_1 and the aa_3 oxidase through the same interaction interface.

Photoinduced Electron Transfer between Ru_z-23-c_{552F} and cyt c_{1CF}. The ruthenium flash photolysis method was used to study the fast ET reaction between cyt c_{1CF} and cyt c_{552F}. This method has previously been applied to characterize both intracomplex and bimolecular ET between various redox partners with microsecond time resolution (*32, 34, 35, 39*). To study the ET reaction between cyt c_{1CF} and cyt c_{552F} in the physiological direction, Ru_z-23-c_{552F} was prepared by

Scheme 1

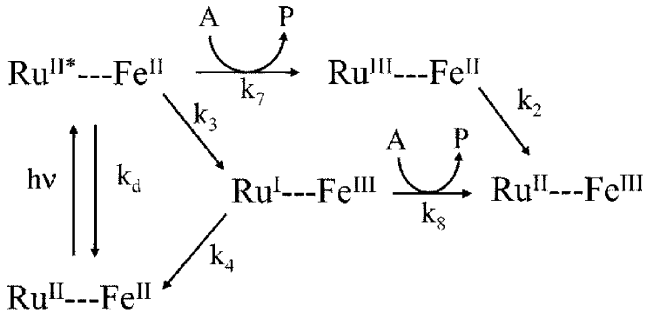

covalently attaching the photoexcitable ruthenium compound Ru(2,2′-bipyrazine)$_2$(4-bromomethyl-4′-methyl-2,2′-bipyridine) (Ru_z) (*3*) to the single cysteine introduced on the surface of cyt c_{552F} (N23C c_{552F}). In this position, the ruthenium complex is on the periphery of the heme crevice surface domain (Figure 1), and there should not be significant steric interference during formation of the ET complex. The second-order rate constant for the reaction between Ru_z-23-c_{552F} and cyt c_{1CF} was $(2.4 \pm 0.3) \times 10^7$ M^{-1} s^{-1} at 8 °C and an ionic strength of 200 mM, compared to a value of $(2.5 \pm 0.3) \times 10^7$ M^{-1} s^{-1} for unlabeled cyt c_{552F} measured by stopped-flow spectroscopy under the same conditions. These results indicate that the ruthenium label does not affect the reaction with cyt c_{1CF} at high ionic strengths. It is possible that the ruthenium complex might affect the reaction at low ionic strengths, which cannot be assessed because the kinetics of wild-type cyt c_{552F} cannot be measured below 50 mM. The +2 charge on the ruthenium complex might strengthen the electrostatic interaction with cyt c_{1CF} at low ionic strengths, favoring complex formation.

The Ru_z complex was designed to measure rapid electron transfer from cyt c_{1CF} to Ru_z-23-c_{552F} in the physiological direction (*35*) (Scheme 1). The driving force of the Ru_z(II*)−Fe(II) → Ru_z(I)−Fe(III) reaction (1.0 V) is close to the expected reorganization energy (λ) of 0.8 V for electron transfer, allowing a maximal rate of electron transfer (*35*). Laser excitation of a solution containing 5.3 μM reduced cyt c_{1CF} and 4.9 μM reduced Ru_z-23-c_{552F} in 10 mM Tris-HCl (pH 8.0) resulted in rapid oxidation of heme *c* Fe(III) by photoexcited Ru_z(II*) in Ru_z-23-c_{552F} (Scheme 1), as indicated by the initial decrease in the 550 nm absorbance (Figure 3). Paraquat was present in the solution to reoxidize Ru(I) (k_8) and prevent the thermal back reaction (k_4) in Scheme 1. The initial rapid decrease in the 550 nm absorbance was followed by an exponential increase with a rate constant of 15000 ± 3000 s^{-1}, indicating electron transfer from cyt c_{1CF} Fe(II) to heme Fe(III) in Ru_z-23-c_{552F}. The oxidation of cyt c_{1CF} with the same rate constant was observed directly at 558 nm, an isosbestic point for cyt c_{552F} (Figure 3). The observed rate constant for electron transfer between cyt c_{1CF} and Ru_z-23-c_{552F} increased linearly as the reduced cyt c_{1CF} concentration increased from 1.6 to 16.7 μM, indicating second-order kinetics with a second-order rate constant (k_{12}) of $(3.1 \pm 0.5) \times 10^9$ M^{-1} s^{-1} (Figure 4). Ascorbate and TMPD were used to keep the cytochromes reduced before flashing. At very low ionic strengths, it was not possible to fully reduce cyt c_{1CF} and some of its variants (which can also be deduced from the redox potentials; see Supplement 2 of the Supporting Information). For this reason, we continuously checked the reduction state of the cytochromes during the experiments by frequently recording absorption spectra to determine the concentration of reduced cyt c_{1CF} for calculating k_{12}. There was no indication of intracomplex electron transfer at the lowest ionic strength examined (10 mM), which would have exhibited an observed rate constant that was independent of protein concentration. The results are consistent with Scheme 2 with an equilibrium dissociation constant K_d (k_d/k_f) of >30 μM. The second-order rate constant (k_{12}) had a very weak dependence on ionic strength from 10 to 35 mM and then decreased rapidly with further increases in ionic strength (Figure 5). A Brønsted plot of log k_{12} versus the square root of the ionic strength was nearly linear in the ionic strength range from 40 to 300 mM, with a Z_AZ_B parameter of −4.85 (Figure 5). The reaction at an ionic strength of >40 mM can thus be described as a diffusional process mediated by long-range

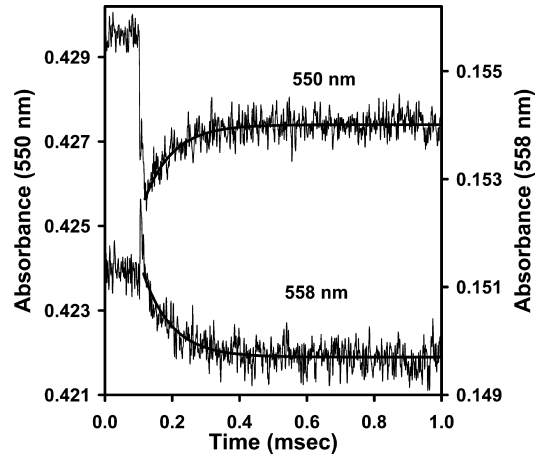

FIGURE 3: Photoinduced electron transfer between WT cyt c_{1CF} and Ru_z-23-c_{552F}. A solution containing 5.3 μM cyt c_{1CF} and 4.9 μM Ru_z-23-c_{552F} in 10 mM Tris-HCl buffer (pH 8.0), 100 μM ascorbate, 1 mM paraquat, and 2 μM TMPD at 25 °C was excited with a 480 nm laser flash with a duration of 0.5 μs. Cytochrome c_{552F} oxidation and re-reduction by cytochrome c_{1CF} were monitored at 550 nm, and cytochrome c_{1CF} oxidation was monitored at 558 nm. The sharp upward spike in the 558 nm transient is due to a light scattering artifact. The rate constant for the exponential transients at both wavelengths is 15000 s^{-1}.

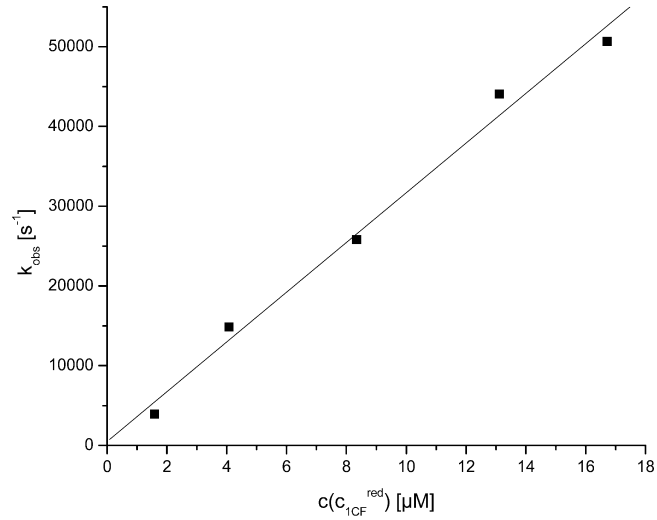

FIGURE 4: Concentration dependence of photoinduced electron transfer between WT cyt c_{1CF} and Ru_z-23-c_{552F}. The conditions were the same as in Figure 3 except that the cyt c_{1CF} concentration was varied from 1.6 to 16.7 μM. The slope of the plot yielded a second-order rate constant (k_{12}) of 3.1×10^9 M^{-1} s^{-1}.

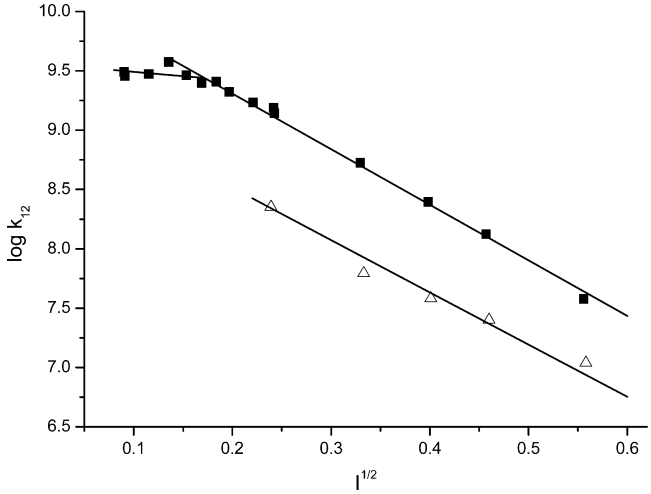

FIGURE 5: Ionic strength dependence of second-order rate constants for the photoinduced electron transfer between WT cyt c_{1CF} and Ru_z-23-c_{552F} (■) and for electron transfer between cyt c_{1CF} and WT cyt c_{552F} measured by stopped-flow spectroscopy (△). The conditions for photoinduced electron transfer were the same as in Figure 3, with KCl added to increase the ionic strength. The stopped-flow spectroscopy experiments involving wild-type cyt c_{552F} were conducted at 8 °C.

Scheme 2

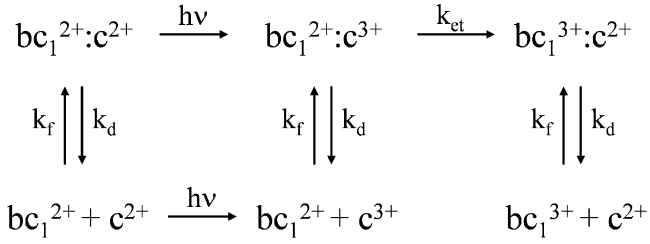

electrostatic interactions. The ionic strength-independent phase of the bimolecular reaction below 40 mM has not been observed before in other rapid kinetic studies of cytochromes. We propose that at ionic strengths of <40 mM, the diffusion process mediated by long-range electrostatic interactions becomes so fast that the second-order rate constant becomes rate-limited by short-range diffusion along the protein surfaces mediated by hydrophobic interactions and is thus not affected by ionic strength. The observation of two phases in the ionic strength dependence of the reaction provides additional evidence of a two-step model of the ET reaction. A similar phenomenon is observed at low ionic strengths in the steady state V_{max}/K_M parameter of some of the reactions of cyt *c* with its redox partners, including bovine and *R. sphaeroides* cyt bc_1 (*17*), cytochrome oxidase (*50*), and cytochrome *c* peroxidase (*32*).

Photoinduced Electron Transfer between Yeast Ru_z-39-Cc and cyt c_{1CF}. The reaction between yeast Ru_z-39-*Cc* and cyt c_{1CF} was also studied to provide a comparison with the reaction between Ru_z-39-*Cc* and yeast cytochrome bc_1 which has been characterized (*35*) with reference to the yeast *Cc*−cyt bc_1 crystal structure (*9*). Laser excitation of a solution containing 5 μM Ru-39-*Cc* and 5 μM cyt c_{1CF} in 5 mM sodium phosphate (pH 7.0) led to electron transfer from the heme Fe(II) in cyt c_{1CF} to the photooxidized heme Fe(III) in Ru_z-39-*Cc* with a rate constant of 50000 s^{-1} observed in both the 550 nm transient for heme *c* and the 557 nm transient for heme c_1 (Figure 6). The observed rate constant was

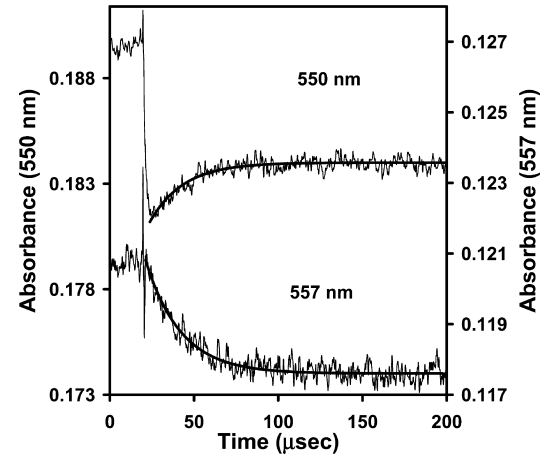

FIGURE 6: Photoinduced electron transfer between WT cyt c_{1CF} and yeast Ru-39-*Cc*. A solution containing 5 μM cyt c_{1CF} and 5 μM Ru_z-39-*Cc* in 5 mM sodium phosphate (pH 7.0), 100 μM ascorbate, and 2 μM TMPD was excited with a 480 nm laser flash with a duration of 0.5 μs. Ru-39-*Cc* photooxidation and re-reduction were monitored at 550 nm, and cyt c_{1CF} oxidation was monitored at 557 nm.

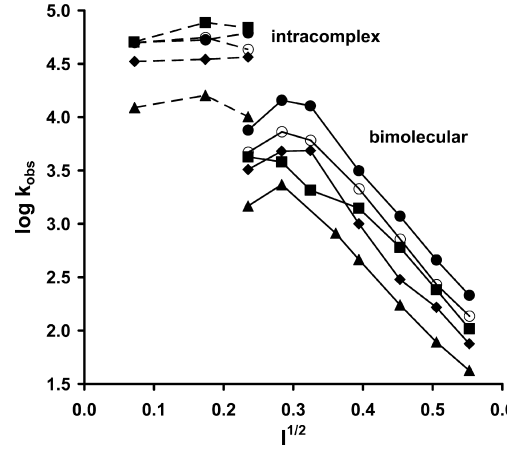

FIGURE 7: Ionic strength dependence of photoinduced electron transfer between Ru_z-39-*Cc* and WT cyt c_{1CF} and its mutants. Solutions contained 10 μM cyt c_{1CF} and 5 μM Ru_z-39-*Cc* in 5 mM sodium phosphate (pH 7.0), 100 μM ascorbate, 2 μM TMPD, and 0−300 mM NaCl at 25 °C: WT c_{1CF} (●), S378A (○), K315E (◆), A247N (■), and E243K (▲). The top curves at low ionic strengths are intracomplex rate constants, while the bottom curves at higher ionic strengths are k_{obs} values for the bimolecular reactions.

independent of protein concentration above 5 μM, indicating intracomplex electron transfer between the two proteins according to Scheme 2 with a K_d (k_d/k_f) of <1 μM. The intracomplex rate constant remained nearly the same as the ionic strength was increased from 10 to 60 mM; however, the amplitude of the intracomplex phase decreased as the complex dissociated, and a new slow phase appeared due to the bimolecular reaction between solution Ru_z-39-*Cc* and cyt c_{1CF}, consistent with Scheme 2 (Figure 7). The relative amplitudes of the intracomplex and bimolecular phases were 69 and 31%, respectively, at an ionic strength of 60 mM, indicating an equilibrium dissociation constant K_d (k_d/k_f) of 2.9 μM for the complex. The rate constant of the bimolecular phase initially increased as the ionic strength was increased from 60 to 80 mM, indicating that the concentration of uncomplexed cyt c_{1CF} increased over this range. At higher ionic strengths, the complex was fully dissociated and the rate constant decreased rapidly, indicating a diffusion process

mediated by long-range electrostatic interactions. The Brønsted Z_AZ_B parameter was −7.3.

The interaction between yeast Ru_z-39-*Cc* and cyt c_{1CF} was stronger than that involving Ru_z-23-c_{552F}, allowing formation of a 1:1 complex at ionic strengths of <70 mM with an intracomplex electron transfer rate constant k_{et} of 50000 s^{-1}. The dissociation constant of the complex, K_d, was 2.9 μM at an ionic strength of 60 mM, and much smaller at lower ionic strengths. In contrast, Ru_z-23-c_{552F} did not form a detectable complex with cyt c_{1CF} at ionic strengths down to 10 mM, and only second-order kinetics could be observed. The Brønsted parameter (Z_AZ_B) was larger for the reaction with Ru_z-39-*Cc* than for that with Ru_z-23-c_{552F}, indicating a stronger electrostatic interaction. In comparison, yeast Ru_z-39-*Cc* and yeast cyt bc_1 form a stable complex at low ionic strengths with an intracomplex ET rate constant of 14000 s^{-1} (*35*), which is independent of ionic strength between 10 and 150 mM, indicating that the complex does not change configuration within this ionic strength range. At ionic strengths of >150 mM, the complex dissociates, and a bimolecular reaction is observed. The reaction between yeast Ru_z-39-*Cc* and the bovine bc_1 complex has intracomplex ET kinetics at ionic strengths of <85 mM with a rate constant of 6300 s^{-1} and becomes bimolecular at ionic strengths of >120 mM (*3*). The reaction between horse Ru-72-*Cc* and *R. sphaeroides* bc_1 reveals intracomplex kinetics at an ionic strength of 85 mM with a rate constant of 6×10^4 s^{-1} and becomes bimolecular at higher ionic strengths (*36*). Thus, the interaction between Ru_z-23-c_{552F} and cyt c_{1CF} is weaker than that of the other systems examined.

Kinetics of the ET Reaction of cyt c_{1CF} Mutants with Ru_z-23-c_{552F} and Ru_z-39-Cc. All cyt c_{1CF} mutants have been examined by the ruthenium photooxidation technique as described above. The effects of the mutations on the reactions with Ru_z-23-c_{552F} and yeast Ru-39-*Cc* were quite similar. The mutations can be clustered into three different regions as indicated in Figure 2. Mutations in regions II and III (A314S, K315T, G319A, S378A, Q381C, and T383C) have relatively little effect on the intracomplex and second-order rate constants or the Z_AZ_B Brønsted parameter (Figures 7−10 and Tables 2 and 3). However, whereas the K315T mutant shows WT behavior, the K315E charge inversion mutant deviates significantly from it. The charge inversion in position 315 leads to a substantial reduction of the second-order rate constants for the reactions with both Ru_z-23-c_{552F} and Ru-39-*Cc* and shows a slight increase in the Z_AZ_B parameter compared to that of WT. The strengthened electrostatic interaction is consistent with the increased negative charge on cyt c_{1CF}, while the decreased rate constant suggests a change in the interaction interface. Mutating position S378, which corresponds to F230 in yeast involved in the cation−π interaction, had little effect. No other aromatic residue in the vicinity of this position could be found in the *Paracoccus* cyt c_1 sequence.

Mutating amino acid positions in region I yielded more significant effects on the kinetics. The charge inversion mutation c_{1CF}E243K decreased the second-order rate constant for the reaction with Ru_z-23-c_{552F} to ~32% of that of the wild type but had a relatively weak effect on the ionic strength dependence (Figure 9 and Table 2). The intracomplex electron transfer rate constant for the reaction with Ru-39-*Cc* was decreased to 12500 s^{-1} by the E243K mutation,

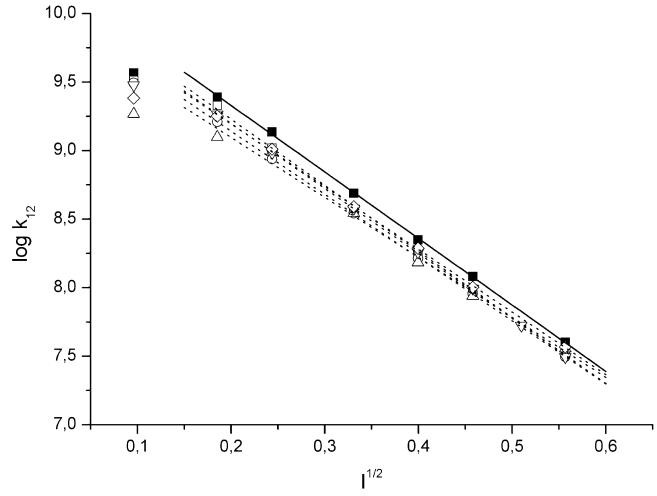

FIGURE 8: Ionic strength dependency of the second-order rate constants (k_{12}) of the ET reaction between WT cyt c_{1CF} and Ru_z-23-c_{552F} compared to cyt c_{1CF} mutants with similar k_{12} values and ionic strength behavior measured by flash photolysis experiments (25 °C): WT c_{1CF} (■), K315T (□), G319A (○), A314S (△), S378A (▽), and Q381V (◇) and (—) fitted Brønsted plot for the bimolecular ET reaction of WT cyt c_{1CF} and (•••) fitted Brønsted plot for the bimolecular ET reaction of cyt c_{1CF} mutants.

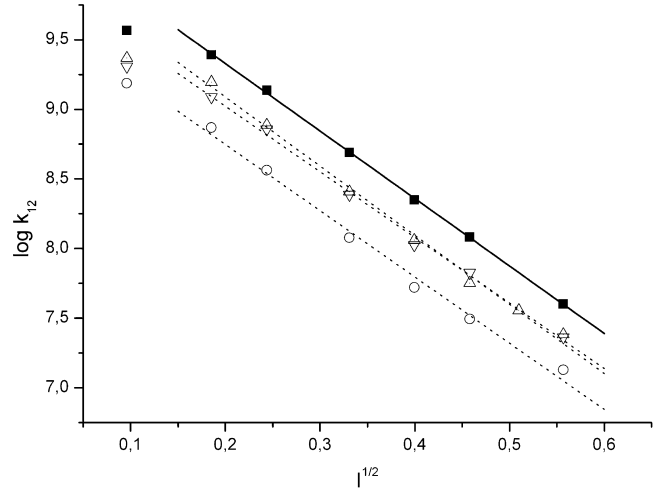

FIGURE 9: Ionic strength dependency of the second-order rate constants (k_{12}) of the ET reaction between WT cyt c_{1CF} and Ru_z-23-c_{552F} compared to mutants with changed k_{12} values but similar ionic strength behavior measured by flash photolysis experiments (25 °C): WT c_{1CF} (■), E243K (△), A247N (○), and T383C (▽) and (—) fitted Brønsted plot for the bimolecular ET reaction of WT cyt c_{1CF} and (•••) fitted Brønsted plot for the bimolecular ET reaction of cyt c_{1CF} mutants.

while the second-order rate constant was decreased to 14% of that of the wild type (Figure 7 and Table 3). This charge inversion mutation appears to significantly alter the orientation of the reactive complex, thus decreasing the rate constants. The A247N mutation in region I decreased the second-order rate constants for the reactions with both Ru_z-23-c_{552F} and Ru-39-*Cc*, indicating an altered reactive complex. The region I mutants V244Q and V244T showed a rather complex effect on the kinetics (Figure 10 and Tables 2 and 3). The V244Q mutation decreased the second-order rate constants for the reactions with Ru_z-23-c_{552F} and Ru-39-*Cc* significantly and slightly decreased the Z_AZ_B parameter for the reaction with Ru_z-23-c_{552F}. The V244T mutation significantly decreased the Z_AZ_B parameter for the reactions with both Ru_z-23-c_{552F} and Ru-39-*Cc* and either decreased

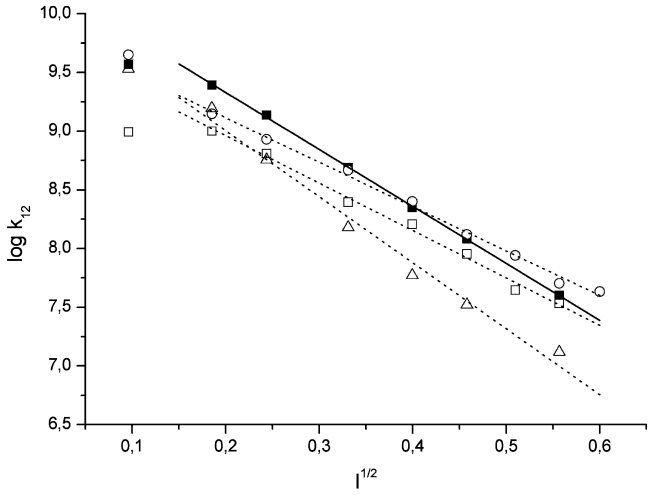

FIGURE 10: Ionic strength dependency of the second-order rate constants (k_{12}) of the ET reaction between WT cyt c_{1CF} and Ru_z-23-c_{552F} compared to mutants with changed k_{12} and ionic strength behavior measured by flash photolysis experiments (25 °C): WT c_{1CF} (■), V244Q (□), V244T (○), and K315E (△) and (—) fitted Brønsted plot for the bimolecular ET reaction of WT cyt c_{1CF} and (•••) fitted Brønsted plot for the bimolecular ET reaction of cyt c_{1CF} mutants.

Table 2: Effect of cyt c_{1CF} Mutants on the Kinetics of Photoinduced ET with Ru_z-23-c_{552F}[a]

cyt c_{1CF}	region	% of WT activity[b]	Z_AZ_B
WT	—	100	−4.85
E243K	I	31−34	−4.95
V244Q	I	47−85	−4.03
V244T	I	62−126	−3.78
A247N	I	60−66	−4.97
A314S	II	75−78	−4.61
K315E	II	17−49	−5.54
K315T	II	86−90	−4.82
G319A	II	84−90	−4.60
S378A	III	78−83	−4.74
Q381V	III	88−93	−4.57
T383C	III	57−62	−4.71

[a] The conditions are the same as in Figure 5. The percent wild-type activity is the percent of the second-order rate constant of the mutant relative to that of the wild type at ionic strengths ranging from 35 to 300 mM. The Brønsted parameter (Z_AZ_B) was determined over this same ionic strength range, and its negative sign implies attractive forces between two oppositely charged partners. [b] Depending on ionic strength conditions.

or increased the rate constant, depending on the ionic strength. Evaluation of the kinetic effects of the V244Q and V244T mutants is complicated by the fact that their redox potentials were decreased to 30 and 139 mV, respectively, compared with 189 mV for WT cyt c_{1CF}. Increasing the bulk and/or the polarity at residue V244 near the heme group while keeping the net charge neutral leads to decreases in the redox potential and complex effects on the kinetics.

Taking these results together, we propose region I as the most effective interaction interface for the ET reaction with cyt c_{552F}. Residues directly contributing to these interactions are those located directly before or within the heme binding motif (E243, V244, and A274). A direct counterpart for F230 of the yeast cytochrome c_1 mediating the cation−π interaction to cyt c (*8*) could not be found in the *Paracoccus* cyt c_1. Since the charge inverting mutations E243K and K315E led to relatively small effects on the ionic strength dependence, the bimolecular reaction between the two cytochromes

Table 3: Effect of cyt c_{1CF} Mutants on the Kinetics of Photoinduced ET with yeast Ru-39-*Cc*[a]

cyt c_{1CF}	region	k_{et} (s^{-1})	k_{12} ($\times 10^8$ M^{-1} s^{-1})	Z_AZ_B
WT	—	50000	3.5 (100%)	−7.3
E243K	I	12500	0.50 (14%)	−6.5
V244Q	I	55000	2.2 (63%)	−7.3
V244T	I	44000	3.7 (106%)	−5.2
A247N	I	55000	1.6 (46%)	−6.7
A314S	II	46000	2.3 (66%)	−7.1
K315E	II	34000	1.1 (31%)	−7.8
K315T	II	38000	3.5 (100%)	−7.3
G319A	II	44000	3.0 (86%)	−6.5
S378A	III	50000	2.2 (63%)	−6.3
Q381V	III	60000	4.1 (117%)	−6.6

[a] The conditions were the same as in Figure 7. The intracomplex electron transfer rate constant (k_{et}) was measured at an ionic strength of 10 mM. The second-order rate constant (k_{12}) was measured at an ionic strength of 160 mM. The Brønsted parameter (Z_AZ_B) was measured at an ionic strength between 100 and 300 mM.

appears to be mediated by long-range electrostatic interactions rather than defined ion pairs, which is in line with the results of Tiede et al. (*25*) and the yeast cytochrome bc_1−c cocrystal data (*7*−*9*).

SUMMARY AND CONCLUSIONS

The ET reaction between *Pd* cyt c_1 and cyt c_{552} was studied using soluble redox fragments of each protein. The new ruthenium derivative Ru_z-23-c_{552F} was designed to measure rapid electron transfer with cyt c_{1CF} in the physiological direction. The second-order rate constant for the ET reaction from cyt c_{1CF} to Ru_z-23-c_{552F} was nearly independent of ionic strength below 40 mM but decreased rapidly with ionic strength above 40 mM. These results are consistent with a two-step model in which the two redox partners first approach each other in a diffusion process mediated by long-range electrostatic interactions, followed by short-range diffusion along the protein surfaces mediated by hydrophobic interactions. The empirical Brønsted parameter (Z_AZ_B) of −4.85 obtained from the ionic strength dependence above 40 mM is similar to that found for the reaction of cyt c_{552F} with the soluble Cu_A fragment of cytochrome c oxidase, strengthening the hypothesis that cyt c_{552} interacts with cyt c_1 via the same interaction interface. The interaction between yeast Ru_z-39-*Cc* and cyt c_{1CF} was stronger than that involving Ru_z-23-c_{552F}, allowing formation of a 1:1 complex at ionic strengths below 70 mM with an intracomplex electron transfer rate constant (k_{et}) of 50000 s^{-1}. The complex dissociated at higher ionic strengths, and the second-order rate constant decreased rapidly with an increase in ionic strength with a Z_AZ_B parameter of −7.3.

To determine the interaction interface on *P. denitrificans* cyt c_1 for cyt c_{552}, a series of cyt c_{1CF} variants in the presumed docking site were prepared with reference to the yeast cyt bc_1−cyt c cocrystal structure (*7*−*9*). Cytochrome c_{1CF} region I (E243, V244, and A247) appears to be the main interaction interface with cyt c_{552F}. Mutations having a significant effect on the kinetics involve residues located directly before or within the heme binding motif (E243, V244, and A247). No direct aromatic counterpart to yeast F230 mediating the cation−π interaction was found in *Paracoccus* cyt c_1. Mutation of cyt c_{1CF} S378, the corresponding residue indicated by the sequence alignment, had no effect on the kinetics.

ACKNOWLEDGMENT

We thank Hans-Werner Müller for excellent technical assistance and acknowledge Maurizio Brunori ("La Sapienza" University, Rome, Italy) for making the stopped-flow apparatus available for us.

SUPPORTING INFORMATION AVAILABLE

Redox difference spectra of cyt c_{1CF} compared to that of selected mutants (Supplement 1), extinction coefficients, DSC wavelengths, and redox potentials of cyt c_{1CF} and its variants (Supplement 2), and sequence alignment of *Pd* cyt c_1 with those of *S. cerevisiae*, *R. capsulatus*, *R. sphaeroides*, and *B. taurus* (Supplement 3). This material is available free of charge via the Internet at http://pubs.acs.org.

REFERENCES

1. Mitchell, P. (1961) Coupling of phosphorylation to electron and hydrogen transfer by a chemi-osmotic type of mechanism. *Nature 191*, 144–148.
2. Gabellini, N., Bowyer, J. R., Hurt, E., Melandri, B. A., and Hauska, G. (1982) A cytochrome b/c_1 complex with ubiquinol-cytochrome c_2 oxidoreductase activity from *Rhodopseudomonas sphaeroides* GA. *Eur. J. Biochem. 126* (1), 105–111.
3. Engstrom, G., Rajagukguk, R., Saunders, A. J., Patel, C. N., Rajagukguk, S., Merbitz-Zahradnik, T., Xiao, K., Pielak, G. J., Trumpower, B., Yu, C. A., Yu, L., Durham, B., and Millett, F. (2003) Design of a ruthenium-labeled cytochrome c derivative to study electron transfer with the cytochrome bc_1 complex. *Biochemistry 42* (10), 2816–2824.
4. Iwata, S., Lee, J. W., Okada, K., Lee, J. K., Iwata, M., Rasmussen, B., Link, T. A., Ramaswamy, S., and Jap, B. K. (1998) Complete structure of the 11-subunit bovine mitochondrial cytochrome bc_1 complex. *Science 281* (5373), 64–71.
5. Berry, E. A., Guergova-Kuras, M., Huang, L. S., and Crofts, A. R. (2000) Structure and function of cytochrome bc complexes. *Annu. Rev. Biochem. 69*, 1005–1075.
6. Hunte, C., Koepke, J., Lange, C., Rossmanith, T., and Michel, H. (2000) Structure at 2.3 Å resolution of the cytochrome bc(1) complex from the yeast *Saccharomyces cerevisiae* co-crystallized with an antibody Fv fragment. *Structure 8* (6), 669–684.
7. Hunte, C., Solmaz, S., and Lange, C. (2002) Electron transfer between yeast cytochrome bc_1 complex and cytochrome c: A structural analysis. *Biochim. Biophys. Acta 1555* (1−3), 21–28.
8. Lange, C., and Hunte, C. (2002) Crystal structure of the yeast cytochrome bc_1 complex with its bound substrate cytochrome c. *Proc. Natl. Acad. Sci. U.S.A. 99* (5), 2800–2805.
9. Solmaz, S. R., and Hunte, C. (2008) Structure of complex III with bound cytochrome c in reduced state and definition of a minimal core interface for electron transfer. *J. Biol. Chem. 283* (25), 17542–17549.
10. Pelletier, H., and Kraut, J. (1992) Crystal structure of a complex between electron transfer partners, cytochrome c peroxidase and cytochrome c. *Science 258* (5089), 1748–1755.
11. Axelrod, H. L., Abresch, E. C., Okamura, M. Y., Yeh, A. P., Rees, D. C., and Feher, G. (2002) X-ray structure determination of the cytochrome c_2: Reaction center electron transfer complex from *Rhodobacter sphaeroides*. *J. Mol. Biol. 319* (2), 501–515.
12. Wienk, H., Maneg, O., Lücke, C., Pristovsek, P., Löhr, F., Ludwig, B., and Rüterjans, H. (2003) Interaction of cytochrome c with cytochrome c oxidase: An NMR study on two soluble fragments derived from *Paracoccus denitrificans*. *Biochemistry 42* (20), 6005–6012.
13. Muresanu, L., Pristovsek, P., Löhr, F., Maneg, O., Mukrasch, M. D., Rüterjans, H., Ludwig, B., and Lücke, C. (2006) The electron transfer complex between cytochrome c_{552} and the Cu_A domain of the *Thermus thermophilus* ba_3 oxidase. A combined NMR and computational approach. *J. Biol. Chem. 281* (20), 14503–14513.
14. Sarewicz, M., Borek, A., Daldal, F., Froncis, W., and Osyczka, A. (2008) Demonstration of short-lived complexes of cytochrome *c* with cytochrome bc_1 by EPR spectroscopy: Implications for the mechanism of interprotein electron transfer. *J. Biol. Chem. 283*, 24826–24836.
15. Speck, S. H., Ferguson-Miller, S., Osheroff, N., and Margoliash, E. (1979) Definition of cytochrome c binding domains by chemical modification: Kinetics of reaction with beef mitochondrial reductase and functional organization of the respiratory chain. *Proc. Natl. Acad. Sci. U.S.A. 76* (1), 155–159.
16. Rieder, R., and Bosshard, H. R. (1980) Comparison of the binding sites on cytochrome c for cytochrome c oxidase, cytochrome bc_1, and cytochrome c_1. Differential acetylation of lysyl residues in free and complexed cytochrome c. *J. Biol. Chem. 255* (10), 4732–4739.
17. Hall, J., Zha, X. H., Yu, L., Yu, C. A., and Millett, F. (1987) The binding domain on horse cytochrome c and *Rhodobacter sphaeroides* cytochrome c_2 for the *Rhodobacter sphaeroides* cytochrome bc_1 complex. *Biochemistry 26* (14), 4501–4504.
18. Hall, J., Zha, X. H., Yu, L., Yu, C. A., and Millett, F. (1989) Role of specific lysine residues in the reaction of *Rhodobacter sphaeroides* cytochrome c_2 with the cytochrome bc_1 complex. *Biochemistry 28* (6), 2568–2571.
19. Nakai, M., Endo, T., Hase, T., Tanaka, Y., Trumpower, B. L., Ishiwatari, H., Asada, A., Bogaki, M., and Matsubara, H. (1993) Acidic regions of cytochrome c_1 are essential for ubiquinol-cytochrome *c* reductase activity in yeast cells lacking the acidic QCR6 protein. *J. Biochem. 114* (6), 919–925.
20. Ubbink, M., Ejdeback, M., Karlsson, B. G., and Bendall, D. S. (1998) The structure of the complex of plastocyanin and cytochrome f, determined by paramagnetic NMR and restrained rigid-body molecular dynamics. *Structure 6* (3), 323–335.
21. Witt, H., Malatesta, F., Nicoletti, F., Brunori, M., and Ludwig, B. (1998) Cytochrome c-binding site on cytochrome oxidase in *Paracoccus denitrificans*. *Eur. J. Biochem. 251* (1−2), 367–373.
22. Drosou, V., Malatesta, F., and Ludwig, B. (2002) Mutations in the docking site for cytochrome c on the *Paracoccus* heme aa_3 oxidase. Electron entry and kinetic phases of the reaction. *Eur. J. Biochem. 269* (12), 2980–2988.
23. Drosou, V., Reincke, B., Schneider, M., and Ludwig, B. (2002) Specificity of the interaction between the *Paracoccus denitrificans* oxidase and its substrate cytochrome c: Comparing the mitochondrial to the homologous bacterial cytochrome c_{552}, and its truncated and site-directed mutants. *Biochemistry 41* (34), 10629–10634.
24. Maneg, O., Ludwig, B., and Malatesta, F. (2003) Different interaction modes of two cytochrome c oxidase soluble Cu_A fragments with their substrates. *J. Biol. Chem. 278* (47), 46734–46740.
25. Tiede, D. M., Vashishta, A. C., and Gunner, M. R. (1993) Electron-transfer kinetics and electrostatic properties of the *Rhodobacter sphaeroides* reaction center and soluble c-cytochromes. *Biochemistry 32* (17), 4515–4531.
26. Kurowski, B., and Ludwig, B. (1987) The genes of the *Paracoccus denitrificans* bc_1 complex. Nucleotide sequence and homologies between bacterial and mitochondrial subunits. *J. Biol. Chem. 262* (28), 13805–13811.
27. Janzon, J., Eichhorn, A. C., Ludwig, B., and Malatesta, F. (2008) Electron transfer kinetics between soluble modules of *Paracoccus denitrificans* cytochrome c_1 and its physiological redox partners. *Biochim. Biophys. Acta 1777* (3), 250–259.
28. Stonehuerner, J., O'Brien, P., Geren, L., Millett, F., Steidl, J., Yu, L., and Yu, C. A. (1985) Identification of the binding site on cytochrome c_1 for cytochrome c. *J. Biol. Chem. 260* (9), 5392–5398.
29. Turba, A., Jetzek, M., and Ludwig, B. (1995) Purification of *Paracoccus denitrificans* cytochrome c_{552} and sequence analysis of the gene. *Eur. J. Biochem. 231* (1), 259–265.
30. Harrenga, A., Reincke, B., Rüterjans, H., Ludwig, B., and Michel, H. (2000) Structure of the soluble domain of cytochrome c_{552} from *Paracoccus denitrificans* in the oxidized and reduced states. *J. Mol. Biol. 295* (3), 667–678.
31. Witt, H., Malatesta, F., Nicoletti, F., Brunori, M., and Ludwig, B. (1998) Tryptophan 121 of subunit II is the electron entry site to cytochrome c oxidase in *Paracoccus denitrificans*. Involvement of a hydrophobic patch in the docking reaction. *J. Biol. Chem. 273* (9), 5132–5136.
32. Maneg, O., Malatesta, F., Ludwig, B., and Drosou, V. (2004) Interaction of cytochrome c with cytochrome oxidase: Two different docking scenarios. *Biochim. Biophys. Acta 1655* (1−3), 274–281.
33. Mooser, D., Maneg, O., Corvey, C., Steiner, T., Malatesta, F., Karas, M., Soulimane, T., and Ludwig, B. (2005) A four-subunit cytochrome bc_1 complex complements the respiratory chain of *Thermus thermophilus*. *Biochim. Biophys. Acta 1708* (2), 262–274.
34. Wang, K., Mei, H., Geren, L., Miller, M. A., Saunders, A., Wang, X., Waldner, J. L., Pielak, G. J., Durham, B., and Millett, F. (1996)

Design of a ruthenium-cytochrome c derivative to measure electron transfer to the radical cation and oxyferryl heme in cytochrome c peroxidase. *Biochemistry 35* (47), 15107–15119.

35. Sadoski, R. C., Engstrom, G., Tian, H., Zhang, L., Yu, C. A., Yu, L., Durham, B., and Millett, F. (2000) Use of a photoactivated ruthenium dimer complex to measure electron transfer between the Rieske iron-sulfur protein and cytochrome c_1 in the cytochrome bc_1 complex. *Biochemistry 39* (15), 4231–4236.
36. Tian, H., Sadoski, R., Zhang, L., Yu, C. A., Yu, L., Durham, B., and Millett, F. (2000) Definition of the interaction domain for cytochrome c on the cytochrome bc_1 complex. Steady-state and rapid kinetic analysis of electron transfer between cytochrome c and *Rhodobacter sphaeroides* cytochrome bc_1 surface mutants. *J. Biol. Chem. 275* (13), 9587–9595.
37. Arslan, E., Schulz, H., Zufferey, R., Kunzler, P., and Thöny-Meyer, L. (1998) Overproduction of the *Bradyrhizobium japonicum* c-type cytochrome subunits of the *cbb*$_3$ oxidase in *Escherichia coli*. *Biochem. Biophys. Res. Commun. 251* (3), 744–747.
38. Witholt, B., Boekhout, M., Brock, M., Kingma, J., Heerikhuizen, H. V., and Leij, L. D. (1976) An efficient and reproducible procedure for the formation of spheroplasts from variously grown *Escherichia coli*. *Anal. Biochem. 74* (1), 160–170.
39. Schägger, H., and von Jagow, G. (1987) Tricine-sodium dodecyl sulfate-polyacrylamide gel electrophoresis for the separation of proteins in the range from 1 to 100 kDa. *Anal. Biochem. 166* (2), 368–379.
40. Thomas, P. E., Ryan, D., and Levin, W. (1976) An improved staining procedure for the detection of the peroxidase activity of cytochrome P-450 on sodium dodecyl sulfate polyacrylamide gels. *Anal. Biochem. 75* (1), 168–176.
41. Pristovsek, P., Lücke, C., Reincke, B., Ludwig, B., and Rüterjans, H. (2000) Solution structure of the functional domain of *Paracoccus denitrificans* cytochrome c_{552} in the reduced state. *Eur. J. Biochem. 267* (13), 4205–4212.
42. Berry, E. A., and Trumpower, B. L. (1987) Simultaneous determination of hemes a, b, and c from pyridine hemochrome spectra. *Anal. Biochem. 161* (1), 1–15.
43. Brønsted, J. N., and La Mer, V. K. (1924) The activity coefficients of ions in very dilute solutions. *J. Am. Chem. Soc. 46* (3), 555–573.
44. Heacock, D. H., Jr., Liu, R. Q., Yu, C. A., Yu, L., Durham, B., and Millett, F. (1993) Intracomplex electron transfer between ruthenium-cytochrome c derivatives and cytochrome c_1. *J. Biol. Chem. 268* (36), 27171–27175.
45. Schoppink, P. J., Hemrika, W., and Berden, J. A. (1989) The effect of deletion of the genes encoding the 40 kDa subunit II or the 17 kDa subunit VI on the steady-state kinetics of yeast ubiquinol-cytochrome c oxidoreductase. *Biochim. Biophys. Acta 974* (2), 192–201.
46. Thompson, J. D., Higgins, D. G., and Gibson, T. J. (1994) CLUSTAL W: Improving the sensitivity of progressive multiple sequence alignment through sequence weighting, position-specific gap penalties and weight matrix choice. *Nucleic Acids Res. 22* (22), 4673–4680.
47. Peitsch, M. C., Wells, T. N., Stampf, D. R., and Sussman, J. L. (1995) The Swiss-3DImage collection and PDB-Browser on the World-Wide Web. *Trends Biochem. Sci. 20* (2), 82–84.
48. Bates, P. A., Kelley, L. A., MacCallum, R. M., and Sternberg, M. J. (2001) Enhancement of protein modeling by human intervention in applying the automatic programs 3D-JIGSAW and 3D-PSSM. *Proteins Suppl. 5*, 39–46.
49. Lambert, C., Leonard, N., De Bolle, X., and Depiereux, E. (2002) ESyPred3D: Prediction of proteins 3D structures. *Bioinformatics 18* (9), 1250–1256.
50. Smith, H. T., Ahmed, A. J., and Millett, F. (1981) Electrostatic interaction of cytochrome c with cytochrome c_1 and cytochrome oxidase. *J. Biol. Chem. 256* (10), 4984–4990.

BI800932C